Microwave-envelope soliton threshold powers and soliton numbers

J. M. Nash, C. E. Patton, and P. Kabos
Colorado State University, Fort Collins, Colorado 80523
(Received 9 December 1994)

The peak power of 5.8-GHz backward-volume-wave pulses propagated in a 7.2-μm-thick yttrium iron garnet film was measured as a function of input pulse width T_0 from 5.1 to 44 ns and input power from 0.05 to 3.5 W in a two-stripline microwave transducer structure. A threshold input power P_{th} for the onset of a nonlinear response was determined as a function of T_0. The dependence of P_{th} on T_0 followed a clear pattern consistent with theoretical considerations for soliton formation. Plots of P_{th} vs $1/T_0^2$ showed two regions where P_{th} scaled linearly with respect to $1/T_0^2$. The slopes of these two linear regions were in ratio 1:9, as expected from theory. A soliton-number parameter n calculated from the P_{th} data as a function of T_0 showed plateaus at $n=1$, 2, and 3. A one-to-one correlation was found between these calculated values of n and the number of peaks in output pulse profiles. These results demonstrate a simple connection between input pulse width, nonlinear power threshold, and soliton number.

I. INTRODUCTION

Microwave magnetic envelope (MME) solitons in thin yttrium iron garnet (YIG) films were first reported by Kalinikos, Kovshikov, and Slavin[1] later by DeGasperis, Marcelli, and Miccoli,[2] and most recently by Chen and co-workers.[3–5] These investigations were carried out for a variety of experimental conditions which included different magnetic field and propagation directions, different surface spin pinning conditions for the YIG films, and different frequency operation points on the dispersion curve of frequency vs wave number. Even though the experiments were all different, the discussion and analysis in all of the above works depended on the ability to decide when a given output pulse profile corresponded to a propagating soliton.

Two methods have been used for the soliton classification of output pulse characteristics. The first method[1] is based on the shape and peak height of the observed output pulses. In a typical experiment,[1,6] the input pulse width was fixed and the input power was slowly increased from a low power of 0.05 mW to a high power of 50 mW or so. The indication of soliton formation was taken to be in the steepening and narrowing of the output pulse which occurred under suitable conditions. This criterion has several limitations. First, careful observation of output pulse profiles shows that even at low power levels the output pulse can have a solitonlike shape. Second, it is well known that a steepening and narrowing of an output pulse can also occur due to a frequency chirp in the input pulse in combination with dispersion in the medium.[7] Third, this method of identifying a soliton is qualitative in nature and sujective at best.

The second method is based on measurements of the pulse peak output power P_{out} vs the peak input power P_{in} for a given input pulse width T_0.[1,2] The P_{out} vs P_{in} response is linear only at low input powers. When the input power is increased, the response changes and the peak output power begins to increase more rapidly. One may associate the threshold power P_{th} for this increase with the critical power for soliton excitation. Observed dependences of P_{th} on pulse width and film thickness appears to support this identification.[2]

This report is concerned with an extension of the second method discussed above. Detailed P_{out} vs P_{in} measurements were made on a single film over a wide range of input pulse widths. For each input pulse width, a value for P_{th} was determined from the P_{out} vs P_{in} data, as in Ref. 2. The dependence of P_{th} on the input pulse width T_0 followed a pattern consistent with theoretical considerations. First, plots of P_{th} vs $1/T_0^2$ showed two distinct regions where P_{th} scales linearly to $1/T_0^2$. Second, the slopes of these two straight-line regions were in ratio 1:9, the same as one would expect for one- and two-soliton generations. Third, a soliton-number parameter n calculated from the P_{th} data as a function of T_0 showed plateaus at $n=1$, 2, and 3. These plateaus could be correlated with the number of peaks for actual output profiles as well.

II. EXPERIMENT

Figure 1 shows a diagram of the microwave transducer structure used to generate and detect MME pulses. The structure consists of two striplines labeled "input" and "output" which are each connected to narrower stripline transducer sections. The transducers are 4 mm apart. The striplines are etched on the surface of a dielectric substrate with a copper ground plane backing. A narrow rectangular piece of a YIG film grown on a single-crystal gadolinium gallium garnet (GGG) substrate is positioned YIG film side down across the two transducers as shown.

The YIG film used in this work was 1.2 cm long, 0.25 cm wide, and 7.2 μm thick. The transducer connected to the input was used to launch backward volume wave (BVW) wave packets in the YIG film. The carrier frequency of the microwave input pulses was 5.8 GHz. The transducer connected to the output was used for pickup. The signals were analyzed by a Hewlett Packard HP71500A microwave transition analyzer. The entire

 ©1995 The American Physical Society

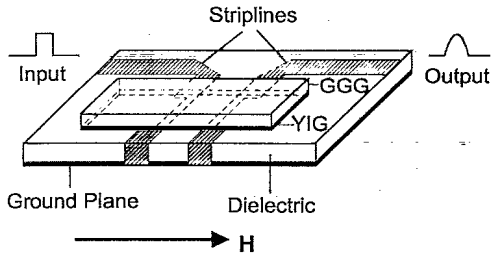

FIG. 1. Diagram of the transducer structure. The structure consists of two striplines on a dielectric substrate with a conducting ground plane backing. Each stripline narrows down to input and output transducer sections. A rectangular yttrium iron garnet (YIG) film on a gadolinium gallium garnet (GGG) substrate is positioned YIG side down over these transducer sections.

structure was oriented so that the external applied magnetic field H was parallel to the in-plane propagation direction from input to output. The field was 1.343 kOe. This value was chosen so that the operating frequency point at 5.8 GHz would lie in the BVW pass band and the coupling between the input microwave signal and low wave-number spin waves would be maximized. The frequency position of the BVW pass band and the operating point will be discussed in more detail below. A more detailed description of the experimental setup and the microwave transducer structure is given in Ref. 3.

Figure 2 shows the applicable main branch BVW dispersion curve of frequency ω vs wave number k for $H=1.343$ kOe and typical YIG parameters. The inset above the dispersion graph shows a wave packet propagating in the BVW configuration parallel to H. The ω vs k plot shows the BVW passband between about 4.0 and 5.9 GHz. The operating point at 5.8 GHz is 100 MHz below the upper edge of the pass band, as indicated by the solid circle on the dispersion curve.

There are several aspects of the BVW dispersion curve in Fig. 2 which are important. First, note that the slope of the curve is maximum for frequencies close to the upper frequency cutoff point at 5.9 GHz. This slope corresponds to the BVW wave-packet group velocity v_g. An operating point close to the cutoff frequency yields the minimum propagation time between input and output transducers as in Fig. 1, for example. This, in turn, minimizes the effects of dissipation and decay on the transmitted pulses. The propagation time for the experiments described above was 124 ns. The corresponding group velocity was 3.2×10^6 cm/s.

Second, note that the operating point is 100 MHz below the 5.9-GHz band edge. This separation is important because of the narrow pulses which are needed for MME soliton experiments, typically down to 5–10 ns in width. Input pulses narrower than 10 ns have a frequency spectrum which is wider than 100 MHz. In the actual experiments, it was found that input pulses below 8 ns in width were filtered by the edge of the BVW band.

Measurements of P_{out} vs P_{in} for each input pulse width were made by varying the input pulse power between a minimum of 0.05 W and a maximum of 3.5 W. The minimum input power was chosen so that measurements made at low input power would be in the linear regime.[3] The maximum input power was determined by the limits of the microwave amplifier used in the experiment. The peak power of the output pulse was recorded at each input power level.

Typical P_{out} vs P_{in} data which demonstrate the nonlinear response are shown in Fig. 3. The solid circles show data obtained for an input pulse width of 19.4 ns. The input power P_{in} for the data in Fig. 3 was varied between 0.15 and 3.2 W. Two important regions in the peak output power response can be seen. The first region corresponds to the low input power range 0.15–1.0 W where the response is linear. The solid line in Fig. 3 is a linear best fit to the P_{out} response in this region. The response changes at $P_{in}\approx1$ W. For input powers above 1.0 W, the peak output power initially shows a second

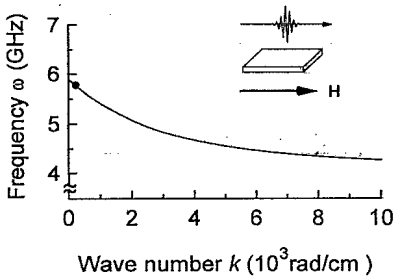

FIG. 2. Dispersion diagram for the backward volume wave (BVW) frequency ω vs wave number k for a static magnetic field H of 1.343 kOe and typical yttrium iron garnet film parameters. The solid circle marks the 5.8-GHz experimental operating point on the dispersion curve. The inset shows a schematic BVW wave packet in the film propagating parallel to the external magnetic field H.

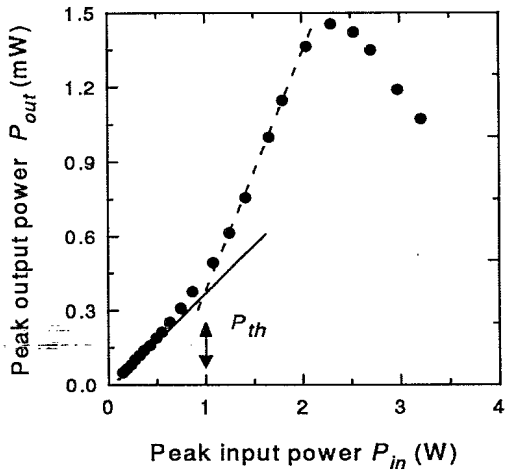

FIG. 3. Typical plot of the peak output power P_{out} vs peak input power P_{in} at a fixed input pulse width of 19.4 ns. The solid circles show the data. The solid line represents a linear best fit to the low input power response. The dashed straight line shows a linear best fit to the more rapid part of the response at higher input powers. The double arrow at P_{th} denotes the input power where the two lines intersect.

linear region, but with a larger slope. The dashed line in Fig. 3 shows a linear best fit to the peak output power response in the second region. The input power level where the solid line and the dashed line intersect is taken as the threshold power P_{th}. It was found that when the input pulse width was greater than about 44 ns the difference in slope between the first region and the second region became very small. This made P_{th} determinations difficult for input pulse widths greater than 38 ns or so. The above intersection procedure was used to determine values of P_{th} for a range of input pulse widths from 5.1 to 44 ns.

III. THRESHOLDS AND SOLITON NUMBERS

Several conditions necessary for the formation of MME solitons can be obtained from theory.[8–10] These conditions are derived, in essence, from solutions of the nonlinear Schrödinger equation. One obtains thresholds for the formation of one or more solitons which depend on the input pulse width, the input pulse power, the spin-wave group velocity, the spin-wave dispersion coefficient, and the spin-wave nonlinearity coefficient. These conditions have been discussed at length in the literature.[3,4,9,11,12]

The condition most often cited for soliton formation is the Lighthill criterion,[13] specified here as $\omega_k'' \cdot N < 0$. The parameter ω_k'' corresponds to the curvature of the $\omega(k)$ vs k dispersion curve in Fig. 2 and is usually defined according to $\omega_k'' = \partial^2\omega(k)/\partial k^2$. The value of ω_k'' for a given wave packet determines how much a given input pulse will spread or disperse as it propagates. The parameter N represents the spin-wave nonlinear response, defined here as $\partial\omega(k)/\partial|u|^2$. The parameter $|u|$ designates the magnitude of the dynamic magnetization response normalized to the saturation magnetization of the material. Specific equations for $|u|$ and $|u|^2$ are developed in Ref. 3. The parameter N describes the effect of BVW amplitude on frequency. When N is large, BVW wave packets of large amplitude will experience a significant shift in frequency.

Solitons may be considered as nonlinear eigenmodes. That is, more and more power or wider pulses do not simply produce bigger solitons; they produce multiple solitons. The condition for soliton formation which is of particular interest here is the threshold power for the production of n solitons, given by[9]

$$|u_0|^2 > \left[\frac{(2n-1)\pi}{2T_0 v_g}\right]^2 \left|\frac{\omega_k''}{N}\right| . \tag{1}$$

The parameter u_0 represents the normalized amplitude of a square pulse initially launched at the input which is to evolve into an n-soliton profile. The quantity $|u_0|^2$ is expected to scale with the input power P_{in}. The effects of each of these parameters on the formation of solitons are discussed in detail in Ref. 3.

It is the functional form of Eq. (1), rather than the detailed formula, which is important here. The form indicates that the threshold power amplitude $|u_0|^2$, or equivalently, the threshold power P_{th}, should scale as $(2n-1)^2/T_0^2$. The parameters in Eq. (1) which are varied during an experiment such as the one described in Sec. II are $|u_0|^2$ and T_0. The input pulse width T_0 is manually controlled by a pulse generator and $|u_0|^2$ is increased by increasing P_{in}. If the linear scaling between P_{in} and $|u_0|^2$ is written as $|u_0|^2 = CP_{in}$, where C is some power scaling factor, Eq. (1) gives an n-soliton input power threshold condition of the form

$$P_{th} = \frac{(2n-1)^2}{T_0^2} A . \tag{2}$$

The multiplier A depends on the various parameters discussed above and the power scaling factor C according to $A = (\pi^2/4v_g^2 C)|\omega_k''/N|$.

Equation (2) constitutes a useful empirical connection between the threshold power P_{th} at which a given soliton signal should begin to form and the number of solitons n which should eventually make up that signal. Note that the factor A will remain fixed for a given operating point. The threshold power, therefore, should simply scale with $1/T_0^2$ and with a P_{th} vs $1/T_0^2$ slope which increases according to $(2n-1)^2$, depending on the soliton number parameter n. When only one soliton is excited, for example, the slope would be equal to A. When two solitons are excited, the slope of the response would be equal to $9A$, or nine times larger than the response associated with one soliton.

The above analysis provides a straightforward way to examine multiple soliton behavior. One simply measures P_{th} vs T_0, plots the data in a P_{th} vs $1/T_0^2$ format, looks for linear regions, and compares slopes. Given the anticipated ratio of 1:9 for the slopes of the initial and second regions, one can also use the initial slope as a calibration point which corresponds to $n=1$ and use P_{th} data to evaluate a soliton number n vs pulse width T_0. The results of such analysis are given below.

IV. EMPIRICAL SOLITON NUMBERS

Figure 4 shows two data plots in the P_{th} vs $1/T_0^2$ format discussed above. The smallest value of $1/T_0^2$ at 0.0005 ns^{-2} corresponds to $T_0 = 44$ ns. The largest value of $1/T_0^2$ at 0.038 ns^{-2} corresponds to $T_0 = 5.1$ ns. The upper plot in (a) shows the data over the entire range of the measurements. The lower plot in (b) shows the data for input pulse widths greater than 18 ns only, on an expanded scale. The labels I and II designate two regions in these P_{th} vs $1/T_0^2$ plots which have a more or less linear character. The straight lines show linear best fits to the corresponding data points.

The region-I line is based on the data for $0.006 < 1/T_0^2 < 0.016$ ns^{-2} or $7.8 < T_0 < 12.9$ ns. The two data points at larger $1/T_0^2$ values correspond to $T_0 = 5.1$ and 6.6 ns. These points do not lie on the linear best-fit line. This is due to the filtering effects already discussed. The region-I best fit has a slope of 42.02 W ns^2 and a P_{th} intercept of 0.32 W. The region-II line is based on the data for $0.0009 < 1/T_0^2 < 0.0017$ ns^{-2} or $24 < T_0 < 33.2$ ns. The region-II fit has a slope of 394.21 W ns^2 and a P_{th} intercept of -0.0004 W.

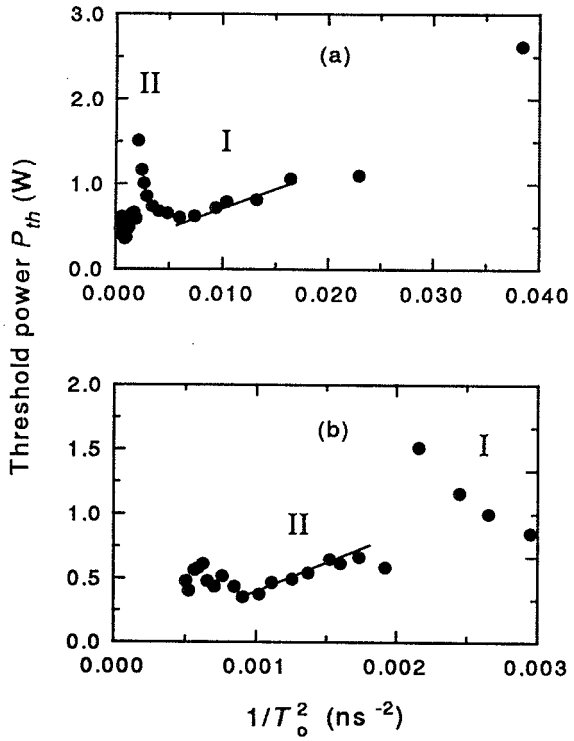

FIG. 4. Plots of power threshold P_{th} vs the inverse of the square of the pulse width, $1/T_0^2$. (a) shows P_{th} vs $1/T_0^2$ for input pulse widths between 7.8 and 45 ns. The line labeled I represents a linear best fit for points between $1/T_0^2=0.006$ and 0.016 ns^{-2}. (b) is a magnification of (a) for $1/T_0^2<0.003$ ns^{-2}. The line labeled II represents a linear best fit for points between $1/T_0^2=0.0009$ and 0.0017 ns^{-2}.

The results in Fig. 4 provide qualitative and quantitative corroboration of the multiple-soliton analysis of Sec. III. The clear pattern of one linear region in the P_{th} vs $1/T_0^2$ data for small T_0, followed by a second linear region for longer T_0 values, is one indication of a soliton response. The ratio of slopes for the region-I and region-II linear best fits provides a further indication of soliton behavior. The anticipated ratio for one- and two-soliton responses, as already noted, is 1:9. The actual ratio from the fitted slopes is 1:9.38. It appears reasonable to associate region I with $n=1$ and to identify region II with $n=2$.

The only discrepancy of note between the data in Fig. 4 and the theory is the non zero value of the P_{th} intercept at $1/T_0^2=0$ for the region-I liner fit. This intercept, at $P_{th}=0.32$ W, is of the same order as the region-I P_{th} values. The region-II intercept at $P_{th}=-0.0004$ W, on the other hand, is close to zero and is consistent with Eq. (2). The origin of the large region-I intercept is not known. It will have a small but distinct effect on the soliton n-parameter analysis presented below.

As indicated in Sec. III, the P_{th} vs T_0 data may be further analyzed to obtain a soliton-number parameter n as a function of input pulse width T_0. This is done by identifying the slope of the region-I linear best fit with the parameter A and then using the P_{th} vs T_0 results in combination with Eq. (2) to determine n vs T_0. The results of this procedure are shown in Fig. 5. The calculated soliton-number parameter n is shown as a function of pulse width T_0, based on the full set of experimental P_{th} vs T_0 determinations for $5.1<T_0<44$ ns, $A=42.02$ W ns^{-2}, and Eq. (2). The horizontal dashed lines at $n=1$, 2, and 3 are intended only as guides to the eye.

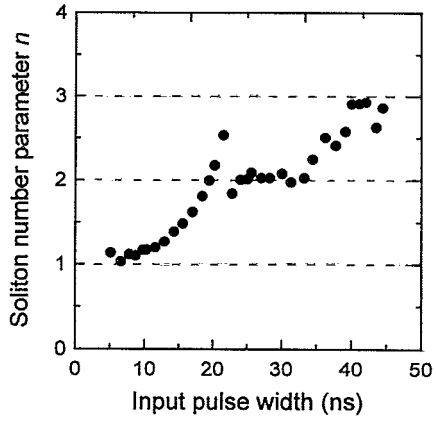

FIG. 5. Plot of soliton-number parameter n vs input pulse width T_0. The solid circles show the calculated soliton-number parameter n as a function of T_0. Dashed horizontal lines are drawn at $n=1$, 2, and 3 as a guide to the eye only.

The results in Fig. 5 show the quantitative correlation between the data and the soliton-number n parameter. The points for the lowest values of T_0 fall, as expected, near $n=1$. This is due to the procedure used to determine the A parameter, based on the slope of the region-I fit in Fig. 4. The fact that these points fall at n values slightly greater than 1 is due to the intercept problem for the region-I linear best fit, as already noted.

As T_0 increases, the Fig. 5 results indicate a gradual increase in the n parameter to a plateau at $n=2$, and then a further increase which approaches a third possible plateau at $n=3$. The plateaus evident in Fig. 5 provide further corroboration of the basic n-soliton threshold dependences embodied in Eq. (2). The widths of the plateaus indicate that there are relatively large ranges of input pulse widths for which a well-defined soliton number n-parameter applies.

The results in Fig. 5. also show that the plateaus with well-defined n values are separated by relatively wide transition regions. The widths of the transitions for both $n=1$ to $n=2$ and $n=2$ to $n=3$ are about 10 ns. A sharp jump in the transition region between $n=1$ and $n=2$, at about $T_0=20$ ns, is evident in Fig. 5 and is a repeatable effect.

The results in Fig. 5 represent a quantitative extension of the soliton number vs pulse width correlations at fixed power reported by Kalinikos, Kovshikov, and Slavin.[14] Those correlations were based on Eq. (1) and visual analysis of output pulse profiles only. Pulse profiles which corroborate the present results are considered below.

It is important to keep in mind that the observation of solitons in the type of experiments described here involves the interplay of various characteristic times which

include the propagation time from input to output, the relaxation time, a dispersion time, and a nonlinear response time. These times are discussed in detail in Ref. 3. The experiments here utilize the input pulse width T_0 as the key control parameter. One effect of increasing T_0 is to reduce the effect of dispersion. This, in turn, increases the time required for a soliton to form. The dispersion time is given in Ref. 3 as $T_d=(v_g^2T_0^2)/|\omega_k''|$. Based on the BVW parameters given in Ref. 3, a 7.2-ns input pulse has a dispersion time of 384 ns and a 44-ns input pulse has a dispersion time of 1430 ns. These dispersion time limits are both substantially larger than the 124-ns propagation time for this experiment. This means that the output pulses which were observed in this experiment do not represent fully formed solitons.

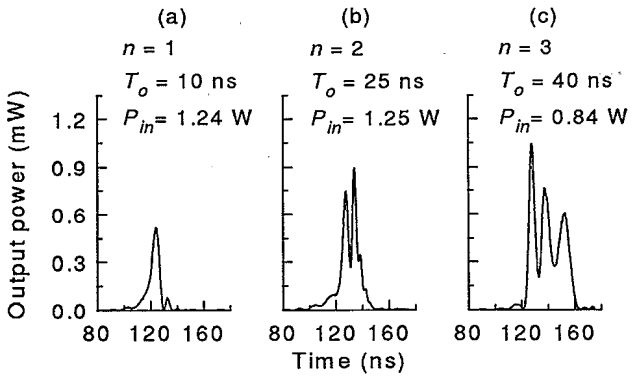

FIG. 6. Output profiles of detected power vs time for three input pulse widths, powers, and soliton numbers as indicated.

V. SOLITON PROFILES

The P_{out} vs P_{in} data analyzed above were obtained from measurements of output pulse profiles. A strong correlation is to be expected between the actual shapes of these profiles and the n values already obtained. An output pulse profile which corresponds to a soliton-number parameter of $n=1$, for example, would be expected to show one main peak, while a profile which corresponds to a soliton number parameter of $n=2$ would have two distinct peaks, and so on. This section presents the results of such a comparison between output pulse profiles and the n values obtained above.

Full output pulse profiles were measured as a matter of course in determining the peak P_{out} values already discussed. Representative above-threshold profiles of output power vs time for the $n=1$, 2, and 3 plateaus are shown in Fig. 6. Figures 6(a)–6(c) are for T_0 values of 10, 25, and 40 ns, respectively. The P_{in} values for these profiles were 1.24, 1.25, and 0.84 W, respectively, roughly twice the applicable P_{th} value in each case.

The profiles in Fig. 6 demonstrate the expected correlations between soliton number and the number of peaks for the given profiles. Figure 6(a), at the $n=1$ plateau, has one peak. Figure 6(b), at the $n=2$ plateau, has two peaks. Figure 6(c), at the $n=3$ plateau, has three peaks. The clear connections between the n values in Fig. 5 and the number of peaks for the profiles in Fig. 6 provide additional support for the soliton-number identifications obtained in the previous section.

VI. SUMMARY AND CONCLUSION

The peak output power P_{out} vs input power P_{in} of backward volume wave microwave magnetic envelope pulses propagating in a thin yttrium iron garnet film has been measured for input pulse widths T_0 in the range 5.1–44 ns. Plots of P_{out} vs P_{in} with T_0 held constant show a linear response at low power and a nonlinear response above some input power threshold P_{th} which changes with T_0.

A simple connection between threshold power, input pulse width, and a soliton-number parameter n is expected from theoretical considerations. These considerations indicate that plots of P_{th} vs $1/T_0^2$ should exhibit several linear regions for which the soliton-number parameter n is constant. Further, the slopes of these regions should scale according to $(2n-1)^2$. Plots of the experimental P_{th} values vs $1/T_0^2$ support these predictions. (1) The P_{th} vs $1/T_0^2$ data show two linear regions for $7.8<T_0<12.9$ ns and for $24<T_0<33.2$ ns. (2) The ratio of the slopes for these regions is 1:9.38, in reasonable agreement with the slope ratio for one- and two-soliton regions. (3) A soliton-number parameter n, evaluated as a function of input pulse width, shows evidence of plateaus close to $n=1$, 2, and 3, respectively. (4) The peak count for the actual output pulse profiles shows good correlation with the soliton n parameters.

These results indicate P_{th} thresholds obtained as a function of pulse width correspond to thresholds for the formation of solitons. These thresholds, moreover, show a systematic connection to a specific number of solitons excited at a given pulse width.

ACKNOWLEDGMENTS

The authors gratefully acknowledge Dr. J. D. Adam of the Westinghouse Research and Development Center, Pittsburgh, Pennsylvania for providing the YIG films used in this experiment. This work was supported in part by the National Science Foundation under Grant Nos. DMR-8921761 and DMR-9400276 and by the U.S. Army Research Office under Grant No. DAAL03-91-G0327.

[1]B. A. Kalinikos, N. B. Kovshikov, and A. N. Slavin, Pis'ma Zh. Eksp. Teor. Fiz. **38**, 343 (1983) [JETP Lett. **38**, 413 (1983)].

[2]P. De Gasperis, R. Marcelli, and G. Miccoli, Phys. Rev. Lett. **59**, 481 (1987).

[3]M. Chen, M. A. Tsankov, J. M. Nash, and C. E. Patton, Phys. Rev. B **49**, 12 773 (1994).

[4]M. Chen, M. A. Tsankov, J. M. Nash, and C. E. Patton, Phys. Rev. Lett. **70**, 1707 (1993).

[5]M. A. Tsankov, M. Chen, and C. E. Patton, J. Appl. Phys. **76**,

4274 (1994).
[6]B. A. Kalinikos, N. B. Kovshikov, and A. N. Slavin, Zh. Eksp. Teor. Fiz. **94**, 159 (1988) [Sov. Phys. JETP **67**, 303 (1988)].
[7]G. P. Agrawal, *Nonlinear Fiber Optics* (Academic, California, 1989).
[8]G. L. Lamb, *Elements of Soliton Theory* (Wiley, New York, 1980).
[9]A. K. Zvezdin and A. F. Popkov, Zh. Eksp. Teor. Fiz. **84**, 606 (1983) [Sov. Phys. JETP **57**, 350 (1983)].
[10]V. E. Zakharov and A. B. Shabat, Zh. Eksp. Teor. Fiz. **61**, 118 (1971) [Sov. Phys. JETP **34**, 62 (1972)].
[11]B. A. Kalinikos, N. G. Kovshikov, and A. N. Slavin, IEEE Trans. Mag. **26**, 5 (1990).
[12]A. N. Slavin and G. M. Dudko, J. Magn. Magn. Mater. **86**, 115 (1990).
[13]M. J. Lighthill, J. Instrum. Math. Appl. **1**, 269 (1965).
[14]B. A. Kalinikos, N. G. Kovshikov, and A. N. Slavin, Fiz. Tverd. Tela **27**, 226 (1985) [Sov. Phys. Solid State **27**, 135 (1985)].